International Journal of Electrical and Computer Engineering (IJECE)
Vol. 9, No. 4, August 2020, pp. xx~xx
ISSN: 2088-8708, DOI: 10.11591/ijece.v9i4.ppxx-xx

A Compact Affordable Electronic Nose Device to Monitor Air Toxic Compounds: A Filter Diagonalization Method Approach

Ricardo Macías-Quijas[1], Ramiro Velázquez[1], Roberto de Fazio[2], Paolo Visconti[2], Nicola I. Giannoccaro[2], Aimé Lay-Ekuakille[2]
[1]Facultad de Ingeniería, Universidad Panamericana, Aguascalientes, Mexico
[2]Department of Innovation Engineering, University of Salento, Lecce, Italy

Article Info

Article history:

Received Jun 9, 2018
Revised Nov 20, 2018
Accepted Jan 11, 2019

Keywords:

Electronic nose (e-nose)
Filter Diagonalization Method
MOS gas sensor
Sensor characterization
Toxic compounds

ABSTRACT

This paper introduces a compact, affordable electronic nose (e-nose) device which aim is to detect volatile compounds that could affect human health, such as carbon monoxide, combustible gas, hydrogen, methane, and smoke, among others. Such artificial olfaction device consists of an array of six metal oxide semiconductor (MOS) sensors and a computer-based system for data acquisition, processing, and visualization. This study further proposes the use of the Filter Diagonalization Method (FDM) to extract the spectral contents of the signals obtained from the sensors. Preliminary results show that the prototype is functional and that the FDM approach is suitable for a later classification stage. Example deployment scenarios of the proposed e-nose include indoor facilities (buildings and warehouses), compromised air quality places (mines and sanitary landfills), public transportation, mobile robots, and wireless sensor networks.

Corresponding Author:

R. Velázquez
Facultad de Ingeniería
Universidad Panamericana
Josemaría Escrivá de Balaguer 101, Aguascalientes, 20290, Mexico.
Email: rvelazquez@up.edu.mx

1. INTRODUCTION

An electronic nose (e-nose) normally consists of a set of different gas sensors that react in a repeatable way when exposed to a wide range of chemical components in the surrounding air space. According to the outputs obtained from the sensors, many conclusions about odor and toxicity can be drawn. E-noses have shown great promise and utility in three domains: food control, disease diagnosis, and environmental monitoring.

E-noses in food control have been devoted toward assuring food quality and safety for human consumption. Some features that e-noses can address in this domain are food freshness, contamination during processing, ageing, shelf life, and authenticity confirmation. Gonzalez-Viejo implemented an e-nose to assess the aroma profiles in beer and automate the industrial quality inspection process [1]. Similarly, Radi developed an e-nose for classifying odors from synthetic flavors such as grapes, strawberry, mango, and orange [2]. With the aim of preventing rancidity, Xu introduced an e-nose monitoring the changes of pecans during storage [3]. Timsorn explored the use of an e-nose device to identify odors from formalin contamination in seafood [4]. To prevent products' adulteration, Gliszczyńska proposed an e-nose to confirm the authenticity of products such as milk, honey, plant oils, and meat [5]. To discourage meat dealers from committing food fraud, Laga presented an e-nose discriminating pork from beef [6]. Wang deployed an e-nose inside a refrigerator to monitor the food freshness level and ageing of fruits, vegetables, and meat [7].

The ability of humans to detect diseases with smell has played a significant role in clinical diagnosis. E-noses can assist in detecting volatile organic compounds (VOC) exhibiting microbial pathogens and have the potential to become a valuable tool in human, animal, and plant disease diagnosis. Sanchez monitored exhaled human breath with an e-nose to assist in the diagnosis of digestive and respiratory diseases [8]. Siyang analyzed the odor of human urine samples with an e-nose to detect diseases such as diabetes [9]. In light of the current pandemic, Airbus is working towards an e-nose prototype capable of sensing COVID-19 in its aircrafts [10]. In the veterinary field, Jia explored an e-nose device for detecting three types of wound infections in rats [11]. To detect bovis-infected cattle in farms, Peled reported the use of an e-nose to analyze VOC in breath samples [12]. In botanics, Baietto explored the use of an e-nose to detect bole-rot fungi that cause wood decay in trees affecting forests [13]. Wilson developed and tested an e-nose for the rapid identification of insecticide residues in crops [14].

Nowadays, e-noses in environmental monitoring have found application in four fields: i) air quality, ii) water quality, iii) process control, and iv) odor control systems [15]. Some representative developments of the above include Wongchoosuk's WiFi e-nose devoted to sense and quantify indoor air contaminants even in very low concentrations [16]. The e-nose prototype proposed by Mishra devoted to identify poison gases emanated from waste [17]. The work of Baby reported on the use of an e-nose to detect the presence of pollutants and pesticides in superficial waters [18]. Iswanto's system, using different gas sensors, was able to monitor gas concentration and temperature in a biogas reactor [19]. The smart system proposed by Ibrahim was capable of sensing ammonium nitrate that could lead to fire and explosion in storage warehouses [20].

Applications of e-noses outside these three main domains also involve explosive detection [21] and the space industry [22].

Within the context of air quality assessment, this paper presents the characterization and implementation of a novel, affordable e-nose device. The prototype consists of a set of six metal oxide semiconductor (MOS) gas sensors capable of detecting i) combustible gas, ii) alcohol, iii) methane, iv) carbon monoxide, v) hydrogen, and vi) smoke, which might represent a threat for the human health. The proposed device exhibits compact dimensions that allow a further and transparent integration into mobile robotic platforms, indoor facilities, public transportation, hazardous places (such as mines and sanitary landfills), or even to be deployed as a set of components in a sensor network to monitor large surface spaces.

Similar e-nose prototypes exploring MOS sensors can be found in the literature [1, 16, 23-25]; sensor arrays range from four to ten, depending on the application. Prototypes rely on MOS technology because it offers small-size and robust sensors, quite good sensitivity, simple signal processing, commercial availability, and low cost. The main difference across devices is the method for data processing. Approaches such as principal component analysis (PCA), artificial neural networks (ANN), Fourier transform, and wavelets have been explored with satisfactory results for further developing predictive models.

In this paper, the sensors' signals were spectrally analyzed using the Filter Diagonalization Method (FDM). To our knowledge, this work is the first one that reports the use of FDM for e-nose data processing.

The remainder of the paper is organized as follows: Section II overviews the e-nose device, the MOS sensors used, the main system components, the FDM, and its implementation in the prototype. In Section III, the experiments that have been carried out are described and the results are shown. Finally, the conclusions and the future work perspectives are given in Section IV.

2. RESEARCH METHOD

An operational prototype was implemented with low-cost materials, and it is the first approach for the research work. The proposed device involves six gas sensors, each one focusing on a specific gas. They capture the components present in the air for later off-line analysis. Additionally, in this first stage, the device encompasses a data acquisition system to visualize the sensors' behaviour, an air pump to convey air samples to the e-nose in an effective manner, and a hermetic acrylic box enclosing the device to ensure a proper gas concentration around the sensors.

2.1. Experimental apparatus

A 3D printed plastic base was designed to host the set of sensors. It exhibits compact dimensions (6.5 cm x 5 cm x 7 cm) and six perforations around its structure to allow a proper installation of the MOS sensors (Figure 1a). All electronic boards and electrical connections are placed inside the structure allowing a clean device and safe prototype handling (Figure 1b).

The prototype employs six different types of MOS sensors (Hanwei Electronics Co., Ltd., Henan, China), which change their electric resistance when its sensing material comes in contact with the gas. Figure 2 illustrates the MOS sensors external and internal structures.

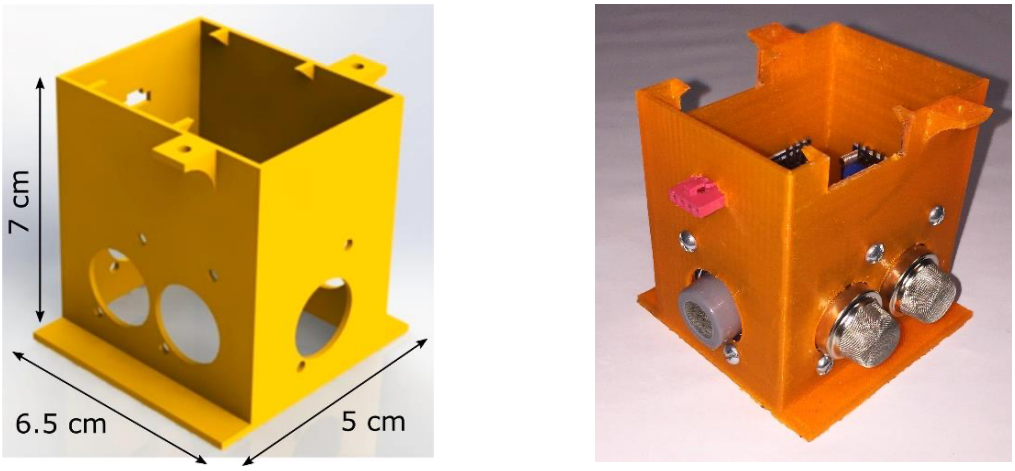

(a) (b)

Figure 1. The plastic base structure: (a) 3D design and (b) actual prototype.

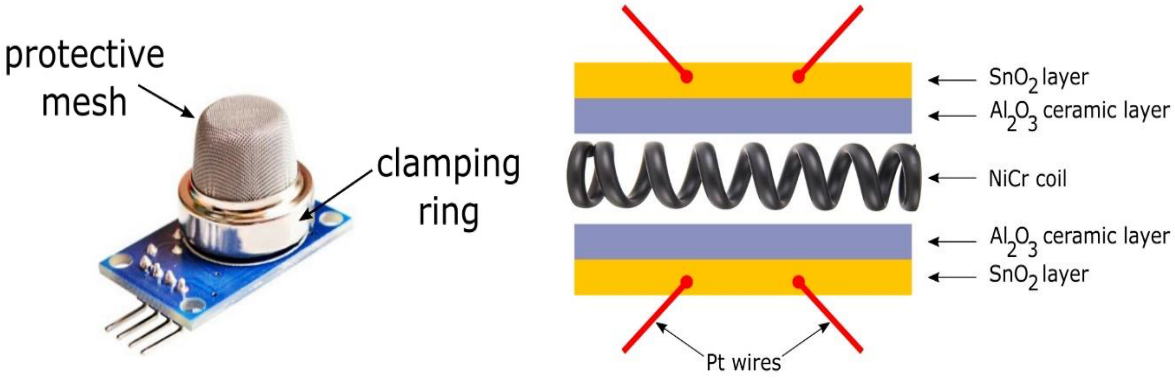

(a) (b)

Figure 2. MOS sensors: (a) external and (b) internal structures.

The external structure (Figure 2a) involves a mesh-like enclosure that protects the sensing material and filters out the suspended particles on the air, so that only gaseous elements access into the chamber. The clamping ring secures the mesh and serves as the base for the sensing material and the electrical connections.

Internally, the sensor is composed of a tin dioxide (SnO_2) layer, which is the sensing material that reacts to the input gas. In clean air, no electric current flows through this layer, but when gas is detected, electrons are released, allowing current to flow. The current output signal is conveyed via platinum (Pt) wires (Figure 2b). Using a simple voltage-divider configuration, the gas concentrations can be derived. Each of the six MOS sensors used in the e-nose prototype focuses on a specific gas providing valuable data upon the analysis of their responses. For this purpose, a complete experimental characterization of sensors' behavior was performed [26]. Three different characteristics were examined: sensitivity, temperature behaviour, and step response. Figure 3 presents, as an example, the behaviour obtained from the alcohol (ethanol) gas sensor (S2). Figure 3a shows its resistance ratio *Rs/Ro*; here, *Rs* represents the sensor resistance to the target gas (C_2H_5OH) given a specific concentration, while *Ro* represents the sensor resistance in clean ambient air. Note that the resistance ratio *Rs/Ro* tends to decrease as the concentration of the gas increases. Figure 3b shows how the sensitivity curve of the sensor is affected by temperature. Here, *Rso* represents the resistance of the sensor in 125 ppm (parts-per-million) alcohol at 20°C. Note that the resistance ratio *Rs/Rso* decreases as environmental temperature increases. Figure 3c shows the sensor response to a step input of 125 ppm alcohol gas. Note that S2 delivers 3.5 V in the presence of the gas and 0.5 V (the baseline) in the absence of gas.

Table 1 summarizes the sensors used in the prototype and their target detection gases. As it can be noticed from Figure 3a and Table 1, each sensor has a main target gas but also detects other secondary gases providing an overlap between the responses of the sensor set. This overlap is desirable since it provides more information about the compounds in the air sample and makes the classification stage easier.

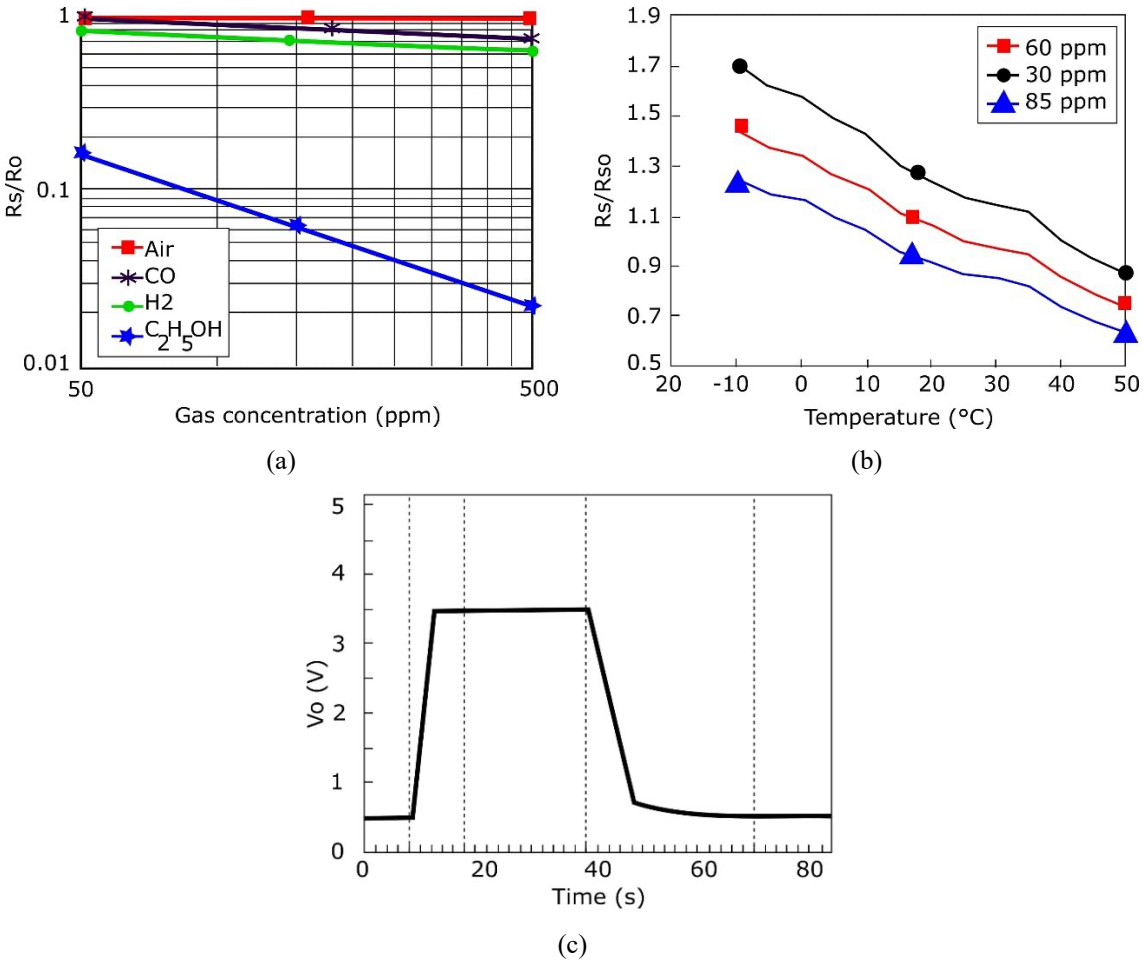

Figure 3. Sensor characterization. Example for S2 (alcohol sensor): (a) sensitivity curve, (b) temperature behaviour, and (c) step response.

Table 1. Sensors used in the e-nose prototype and detected gases.

Sensor	Hanwei item	Target Gas	Detected Gases
S1	MQ2	Combustible gas	H_2, LPG, CH_4, CO, Alcohol, Propane
S2	MQ3	Alcohol	CO, H_2
S3	MQ4	Methane	Propane, Butane, Alcohol
S4	MQ7	Carbon monoxide	H_2, LPG,CH_4
S5	MQ8	Hydrogen	CO
S6	MQ135	Air quality	NH_3, NOx, Alcohol, Benzene, Smoke, CO_2

The e-nose prototype encompasses a data acquisition system and an electronic control unit responsible for capturing and analyzing data.

The electronic unit consists of a 32-bit microcontroller (Texas instruments Stellaris LM4F120) in charge of the air pump control and the sensors' data acquisition with a USB interface to a computer for a later data display and off-line processing. Figure 4a shows the block-level diagram of the system.

Figure 4b shows the electrical diagram for the air pump control and power supply of the system. In addition, a simple communication protocol was implemented between the microcontroller and the computer to synchronize the start and end of data acquisition and transfer the captured data for processing.

Figure 5 shows the activity diagram of the system operation. The process is initiated by the computer and lasts 180 s. During this time, the sensors capture data from the surrounding environment. After 20 s of initiated the process, the pump injects air into the hermetic box for 30 s. The pump is deactivated at t=50 s; the sensors start to reset (i.e. they go to their baseline). The microcontroller captures this behaviour as well. Figure 6 illustrates all six sensors' responses detailing the different stages. Note that the response of S2 (alcohol gas sensor) is the slowest one both in its rising and recovery times. This result is due to the low volatility that alcohol exhibits compared to the other substances explored.

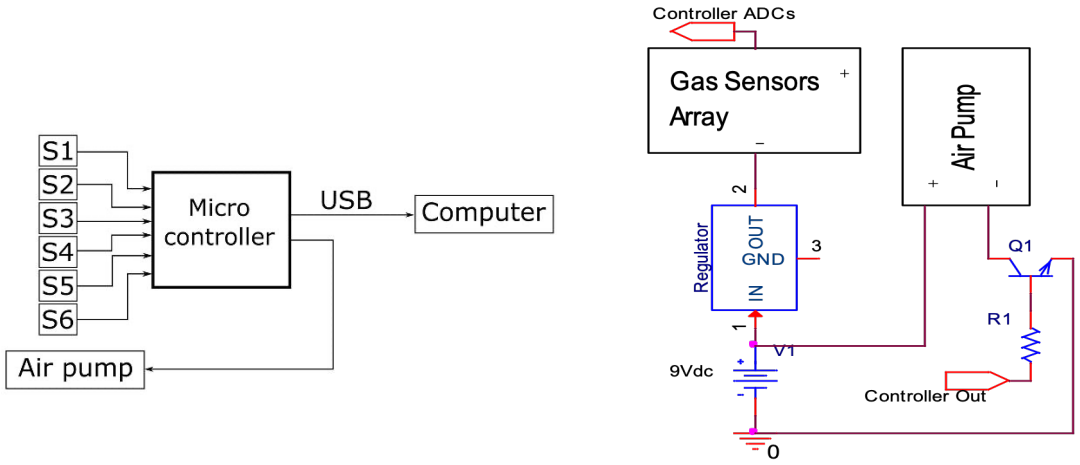

(a) (b)

Figure 4. E-nose system: (a) Block-level diagram and (b) electrical diagram of the power supply and air pump control.

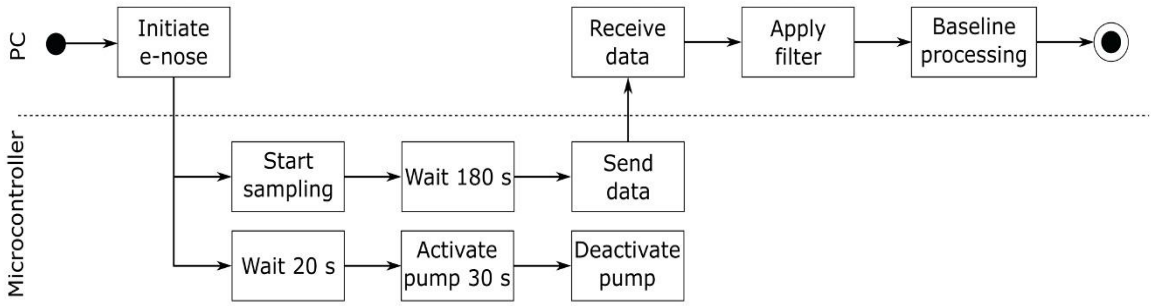

Figure 5. The activity diagram for the e-nose software.

After 180 s, the microcontroller takes the samples from the sensors readings, converts them to digital format, and builds a data frame. The data frame is then transferred to the computer via USB protocol. Once in the computer, samples obtained from each sensor are filtered using a ten-tap moving average filter working as a lowpass filter. The objective of the signal filtering is to avoid undesirable peaks in the response of the sensors, thus providing a smoother output. The final stage consists of determining and eliminating the sensors' individual baselines. The purpose of this step is to obtain reliable curves with real and comparable maximum and minimum points. Equation (1) was used to eliminate the baseline without affecting the curve characteristics.

$$y_i = y_i - y_{i0} \quad (1)$$

where y_i represents the output of the i^{th}-sensor and y_{i0} its baseline. The final prototype is shown in figure 7a. Note that the microcontroller is fitted in the plastic base. The necessary connections between the sensors and the controller are located inside. Figure 7b shows the implemented system. The plastic base with the sensors connected to the microcontroller inside the hermetic box can be seen. Outside the hermetic box, the air pump with a sample input tube and an output tube that goes inside the box can be appreciated. The air pump control and the power supply system are also shown. The final prototype exhibits compact dimensions (see Figure 1a); it is lightweight (500 g) and affordable (150 USD).

2.2. FDM analysis

The Filter Diagonalization Method (FDM) was initially developed for quantum dynamics calculations [27] and later used for Nuclear Magnetic Resonance (NMR) signal processing [28], and leak detection in pipelines [29, 30]. It provides a nonlinear parametric method for time-domain signal analysis using a sum of damped sinusoids.

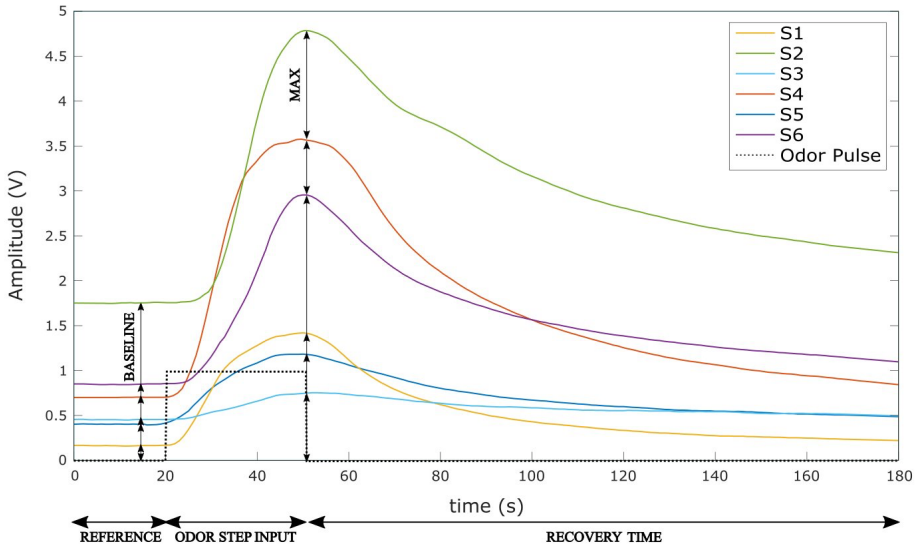

Figure 6. The sensors' response during the acquisition process.

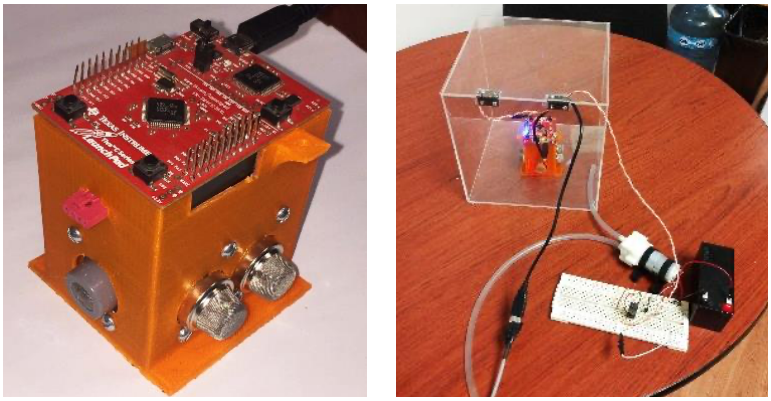

(a) (b)

Figure 7. First prototype: (a) Control unit and sensors in the plastic base. (b) The prototype with the external air pump and the hermetic box.

FDM is traditionally used to solve Harmonic Inversion Problems (HIP), delivering high-resolution spectra. Compared to Fourier analysis, it is not limited by the incertitude principle, thus providing high-quality spectra together with a high signal to noise ratio (SNR) without needing a large number of samples.

2.2.1. FDM formulation

To explain the method, let us consider a complex unidimensional signal $c_n = c(n\tau)$ with values along with equidistant time intervals $n\tau$ with n = 0, 1, …, N-1. The FDM aims to represent c_n as a sum of damped sinusoids, as shown in equation (2), where $\omega_k = 2\pi f_k - j\gamma_k$ are the complex frequencies of the signal, including the damping factor, and d_k are the corresponding amplitudes. To solve equation (1), the FDM associates a correlation function described by the Hamiltonian operator $\hat{\Omega}$, which has complex eigenvalues $\{\omega_k\}$, thus c_n can be further transformed into equation (3):

$$c_n = \sum_{k=1}^{K} d_k e^{-jn\tau\omega_k} \tag{2}$$

$$c_n = \left(\Phi_0 \middle| e^{-jn\tau\Omega} \Phi_0\right) \tag{3}$$

The problem can be simplified to the diagonalization of the Hamiltonian operator $\hat{\Omega}$ or, as discussed in [28], to the evolution operator $\hat{U} = e^{-j\tau\Omega}$. Briefly, a symmetric internal product operator defined by (a|b)=(b|a) without the conjugate complex is used, where Φ_0 is the initial state. Assuming that an orthonormal eigenvector set γ_k is used to perform diagonalization of the evolution operator (equation (4)):

$$\hat{U} = \sum_k u_k |Y_k)(Y_k| = \sum_k e^{-j\omega_k\tau}|Y_k)(Y_k| \tag{4}$$

and substituting (4) in (3), yields equation (5):

$$d_k = (\Phi_0|Y_k)(Y_k|\psi_0) = (Y_k|\Phi_0)^2 \tag{5}$$

The resulting eigenvalues determine the position and width of the harmonics while the eigenvectors define their amplitudes and phases. Assuming a set created from the Krylov vectors, generated by the evolution operator $\Phi_n = U^n\Phi_0 = e^{-jn\tau\hat{\Omega}}\Phi_0$ and according to equation (5), it yields:

$$\left(\Phi_n\middle|\hat{U}\Phi_m\right) = (\Phi_n|\Phi_{m+1}) = c_{m+n+1} \tag{6}$$

As the set in non-orthonormal, the overlapping matrix can be calculated according to equation (7):

$$(\Phi_n|\Phi_m) = \left(\hat{U}^n\Phi_0\middle|U^m\Phi_0\right) = \left(\Phi_0\middle|\hat{U}^{m+n}\Phi_0\right) = c_{m+n+1} \tag{7}$$

Equation (7) is strictly related to the values of the measured signal. Notation $\mathbf{U^0}$ can then be used, being this the overlapping matrix representation of dimensions M+1×M+1. Similarly, $\mathbf{U^1}$ can be used for $\hat{U}$. To reformulate equation (2), it is then necessary to solve the generalized eigenvalues problem. This is (equation (8)):

$$\mathbf{U^1B}_K=u_k\mathbf{U^0B}_k \tag{8}$$

where $u_k = e^{-jn\omega_k\tau}$ contains the lines of the spectrum and its corresponding widths. Eigenvectors $\mathbf{B}_k$ contain both amplitudes and phases.

2.2.2. FDM implementation for the e-nose

With the aim of analyzing the sensors' experimental data, the FDM was implemented. The sensors' readings were used as inputs c_n, and the FDM was used to estimate their spectra. The following steps were performed by the algorithm:

1) Taking into account the Nyquist criterion, the frequency interval [f_{min} f_{max}] in which the spectral analysis of signal c_n will be performed is selected; c_n is sampled at $f_s = \frac{1}{\tau}$.

2) An angular frequency equidistant axis with values $2\pi f_{min}<\varphi j<2\pi f_{max}$, j=0,1,2,…,$K_{win}$ is created. Value K_{win} is chosen as $K_{win} = \frac{N(f_{max}-f_{min})}{2\tau}$ as suggested in the literature.

3) Three symmetric complex matrices $\mathbf{U}^{(p)}$ of dimensions K_{win} x K_{win}, with p = 0, 1, 2 are determined. To calculate the elements that do not belong to the diagonal, equation (9) can be used, where f_p and g_p are the Fourier transforms of the first and second part of signal c_n [31], detailed in equations (10).

$$\boldsymbol{U}^{(p)}(\varphi,\varphi') = \frac{e^{j\varphi}f_p(\varphi') - e^{j\varphi'}f_p(\varphi) + e^{jM\varphi'}g_p(\varphi) + e^{jM\varphi}g_p(\varphi')}{e^{-j\varphi} - e^{-j\varphi'}} \tag{9}$$

$$f_p(\varphi) = \sum_{n=0}^{M} e^{jn\varphi}c_{n+p}$$
$$g_p(\varphi) = \sum_{n=M+1}^{2M} e^{j(n-m-1)\varphi}c_{n+p} \tag{10}$$

Equation (11) is used to calculate the elements located in the diagonal:

$$\boldsymbol{U}^{(p)}(\varphi,\varphi') = \sum_{n=0}^{2M}(M+1-|m-n|)e^{jn\varphi} \tag{11}$$

4) Solve the generalized eigenvalues problem with equation (8), where the eigenvalues and eigenvectors are calculated using the QZ factorization algorithm [32].

5) Select the complex amplitudes d_k using equation (12):

$$d_k^{1/2} = \sum_{j=1}^{K_{win}} \boldsymbol{B}_{jk} \sum_{n=0}^{M} c_n e^{jn\varphi_j} \tag{12}$$

6) Use values ω_k and d_k to estimate the spectrum with equation (13):

$$C(F) = -\sum_k Im\left\{\frac{d_k}{2\pi F - \omega_k}\right\} \tag{13}$$

Figure 8 shows a flowchart summarizing the FDM algorithm implementation.

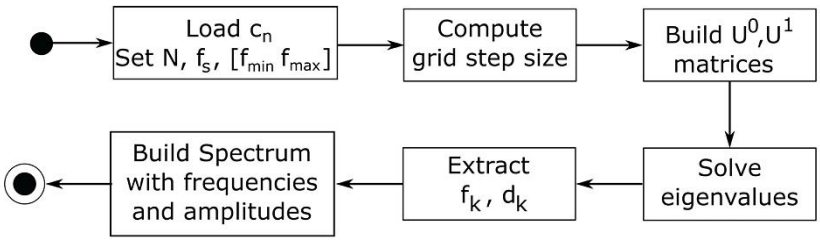

Figure 8. FDM implementation algorithm for the e-nose.

3. RESULTS AND DISCUSSION

3.1. E-nose data processing with FMD

A series of experiments were designed using common gases to test the performance of the device, obtaining some preliminary results that are presented in this Section. The environmental conditions registered during the experiments were a temperature of 23ºC ± 2 ºC and relative humidity (RH) of 30 %. For each experiment, the e-nose was subjected to a gas sample, and two features were obtained:

1) The sensors response in the time domain consisted of a series of 180 samples for each of the six sensors.
2) The frequency spectrum for each sensor response was calculated using the FDM described in Section 2.2. The spectrum of a sensor is given by equation (14):

$$Y_n(f) = \sum_k a_{k,n}\delta(f - f_{k,n}) \tag{14}$$

where f_k and a_k are the frequencies and amplitudes belonging to the k^{th}-harmonic found in the response of the n^{th}-sensor, respectively. The system response to clean air was first verified. As expected, the sensor set showed constant low magnitude output values. The FDM-based spectrum revealed low amplitude peaks and frequencies with inexistent harmonics. It can be therefore concluded that the sensors' response to clean air is negligible. Figure 9 shows the e-nose response to acetone (C_3H_6O). Note in Figure 9 left how the sensors respond to the stimulus represented by the dotted line, especially sensors S4 and S2 followed by S6, this last indicating the air quality. In addition, a spectrum containing harmonics of relevant magnitude in a narrow frequency range can be observed (Figure 9 right). Table 2 summarizes the frequency (Sn_F) and amplitude (Sn_A) values found by the FDM algorithm.

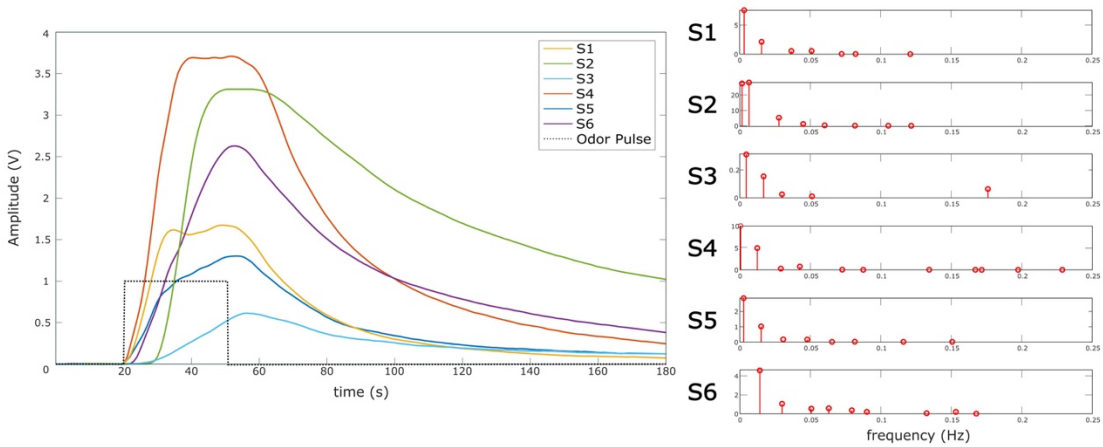

Figure 9. The e-nose response to acetone: (left) time response and (right) FDM-based spectrum.

Table 2. Acetone: amplitude (Sn_A) and frequency (Sn_F) values got for each sensor reading using FDM.

S1 A	S1 F	S2 A	S2 F	S3 A	S3 F	S4 A	S4 F	S5 A	S5 F	S6 A	S6 F
0.039	0.464	27.466	0.001	0.063	0.176	0.012	0.433	2.859	0.003	4.580	0.014
7.571	0.003	28.083	0.006	0.311	0.005	0.016	0.410	1.024	0.015	1.061	0.030
2.132	0.016	5.256	0.028	0.154	0.017	10.011	0	0.178	0.031	0.542	0.051
0.545	0.037	1.195	0.045	0.025	0.030	4.978	0.012	0.166	0.048	0.584	0.063
0.539	0.051	0.322	0.060	0.011	0.051	0.295	0.029	0.015	0.065	0.373	0.079
0.041	0.072	0.110	0.082			0.761	0.042	0.027	0.082	0.206	0.090
0.031	0.082	0.071	0.105			0.058	0.073	0.019	0.116	0.060	0.132
0.011	0.121	0.041	0.122			0.020	0.087	0.016	0.151	0.201	0.153
						0.022	0.229			0.015	0.168
						0.015	0.197				
						0.034	0.134				
						0.014	0.172				
						0.026	0.167				

Figure 10 shows the response to ethanol at 71.5%. Sensors S2 and S4 exhibit the most significant responses (Figure 10 left). Note that S2 shows the highest amplitude value while S4 shows the fastest rise time. Table 3 lists the harmonic values found by the FDM algorithm. Finally, figure 11 shows the e-nose response to gas butane (C_4H_{10}). Note that S4 exhibits the greatest response. Table 4 shows the harmonics found by the FDM analysis.

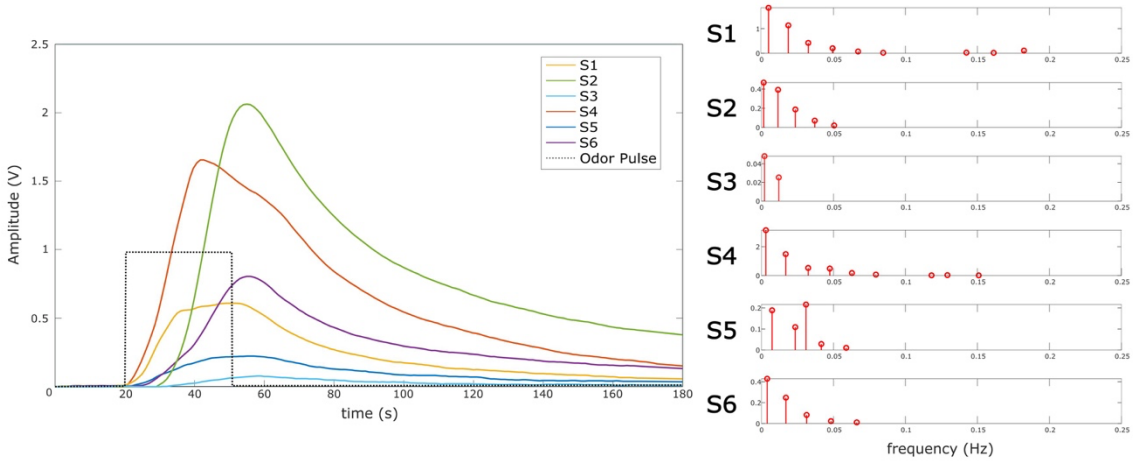

Figure 10. The e-nose response to ethanol: (left) time response and (right) FDM-based spectrum.

Table 3. Ethanol: amplitude (Sn_A) and frequency (Sn_F) values got for each sensor reading using FDM.

S1_A	S1_F	S2_A	S2_F	S3_A	S3_F	S4_A	S4_F	S5_A	S5_F	S6_A	S6_F
0.012	0.423	0.468	0.002	0.048	0.002	3.146	0.003	0.189	0.007	0.428	0.004
1.852	0.005	0.393	0.011	0.025	0.012	1.487	0.017	0.109	0.023	0.248	0.017
1.135	0.019	0.187	0.023			0.531	0.032	0.216	0.031	0.083	0.031
0.421	0.032	0.071	0.037			0.489	0.047	0.029	0.042	0.024	0.048
0.203	0.049	0.021	0.050			0.178	0.063	0.010	0.059	0.012	0.066
0.071	0.067					0.071	0.079				
0.017	0.085					0.018	0.118				
0.108	0.182					0.032	0.129				
0.023	0.142					0.013	0.151				
0.015	0.161										

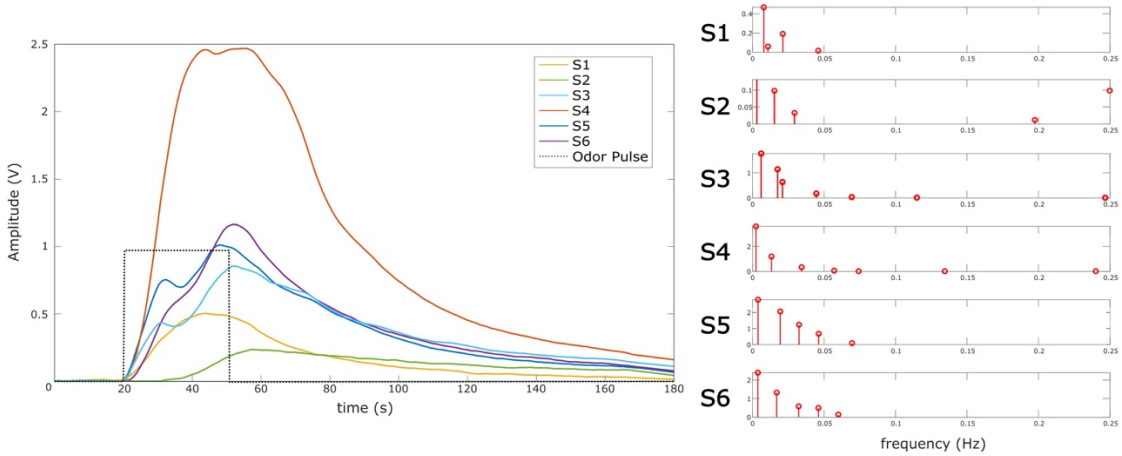

Figure 11. The e-nose response to gas butane: (left) time response and (right) FDM-based spectrum.

Table 4. Gas butane: amplitude (Sn_A) and frequency (Sn_F) values got for each sensor reading using FDM.

S1_A	S1_F	S2_A	S2_F	S3_A	S3_F	S4_A	S4_F	S5_A	S5_F	S6_A	S6_F
0.060	0.011	0.131	0.003	1.760	0.006	3.603	0.002	2.782	0.004	2.388	0.004
0.467	0.008	0.098	0.015	1.136	0.017	1.191	0.013	2.049	0.019	1.322	0.017
0.191	0.021	0.033	0.029	0.632	0.021	0.333	0.034	1.230	0.033	0.581	0.032
0.017	0.046	0.012	0.197	0.175	0.045	0.056	0.057	0.677	0.046	0.496	0.046
				0.036	0.069	0.014	0.074	0.095	0.070	0.140	0.060
				0.015	0.115	0.016	0.240				
				0.010	0.247	0.014	0.134				

3.2. Comparison with Fourier analysis

The Discrete Fourier Transform (DFT) is the most commonly used method to solve the Harmonic Inversion Problem (HIP) using the reliable and efficient Fast Fourier Transform (FFT) algorithm. However, the FFT is sensitive to time-frequency uncertainties which limit the resolution of the resulting spectrum. As the FFT spectrum resolution depends on the number of processed samples, the use of excessively large data sets is often necessary. In contrast, the FDM is a parametric method that, upon the use of linear algebra, extracts the parameters relevant for the construction of the signal spectrum. The FDM outperforms the FFT as it requires a lower amount of data to build the spectrum and does not restrain the spectrum resolution with uncertainties. Figure 12 compares the FDM and FFT spectra for the acetone sample. The comparison is limited to the signals of sensors S2 and S4, which show the clearest response to acetone. Note that the FDM produces more accurate high-resolution spectra with well-defined peaks. Harmonics are well separated among them, clearly showing the signal frequencies in the spectrum. In contrast, the FFT produces wide peaks that tend to merge between them; this low-resolution effect might lose or miss information on the spectrum harmonics. Note that the FDM-based spectrum exhibits a higher number of harmonics represented by well-defined peaks. It can be therefore concluded that the FDM-based spectrum is a clearer and more accurate representation for the e-nose signal processing.

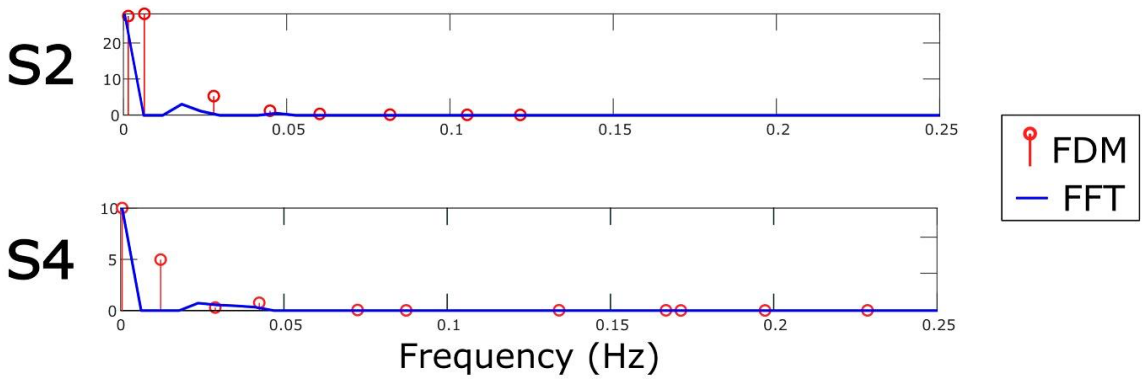

Figure 12. Performance comparison between FDM and FFT (180 samples).

4. CONCLUSION

This paper has presented a self-developed e-nose device built with low-cost components which aim is to detect possible toxic compounds in the ambient air. The prototype encompasses a set of six MOS gas sensors, a data acquisition system, and a computer-based interface for data visualization and analysis. At this point, the hardware design and functional testing stages have concluded, fulfilling the requirements and yielding satisfactory results. MOS sensors offer small size, low power consumption, fast response, and recovery times. Their response can be divided in three time-regions: the reference value (baseline), the rising time, and the resetting time.

The Filter Diagonalization Method (FDM) was implemented to calculate the harmonics involved in the acquired signals. The algorithm showed high precision using a low number of samples. To our knowledge, FDM has not been previously explored for e-nose data processing. The spectra of the sensors' responses were obtained.

Current work focuses on using these spectra to perform gas classification. Approaches such as Random Forest [33] and Convolutional Neural Networks (CNN) [34] are currently being considered. Future work will evaluate the possibility of optimizing the number of sensors while keeping satisfactory results and migrating the electronic unit to an FPGA SoC architecture [35]. Applications in wireless sensor networks (WSN) for intelligent buildings [36] and farms [37] are foreseen.

REFERENCES

[1] C. Gonzalez-Viejo, S. Fuentes, A. Godbole, B. Widdicombe, R.R. Unnithan, "Development of a Low-Cost e-nose to Assess Aroma Profiles: An Artificial Intelligence Application to Assess Beer Quality," *Sensors and Actuators B: Chemical*, vol. 308, pp. 1-7, 2020.

[2] R. Radi, B. Barokah, D.N. Rohmah, E. Wahyudi, M.D. Adhityamurti, J.P. Putro, "Implementation of an Electronic Nose for Classification of Synthetic Flavors," *Bulletin of Electrical Engineering and Informatics*, vol. 10, no. 3, pp. 1283-1290, 2021.

[3] K. Xu, J. Wang, Z. Wei, F. Deng, Y. Wang, S. Cheng, "An Optimization of the MOS Electronic Nose Sensor Array for the Detection of Chinese Pecan Quality," *Journal of Food Engineering*, vol. 203, pp. 25-31, 2017.

[4] K. Timsorn, C. Wongchoosuk, "Inkjet Printing of Room-Temperature Gas Sensors for Identification of Formalin Contamination in Squids," *Journal of Materials Science: Materials in Electronics*, vol. 30, pp. 4782-4791, 2019.

[5] A. Gliszczyńska-Świglo, J. Chmielewski, "Electronic Nose as a Tool for Monitoring the Authenticity of Food: A Review," *Food Analytical Methods*, vol. 10, pp. 1800-1816, 2017.

[6] S.A. Laga, R. Sarno, "Temperature Effect of Electronic Nose Sampling for Classifying Mixture of Beef and Pork," *Indonesian Journal of Electrical Engineering and Computer Science*, vol. 19, no. 3, pp. 1626-1634, 2020.

[7] M. Wang, F. Gao, Q. Wu, J. Zhang, Y. Xue, H. Wan, P. Wang, "The Real-time Assessment of Food Freshness in Refrigerator Based on Miniaturized Electronic Nose," *Analytical Methods*, vol. 10, pp. 4741-4749, 2018.

[8] C. Sanchez, J.P. Santos, J. Lozano, "Use of Electronic Noses for Diagnosis of Digestive and Respiratory Diseases through the Breath," *Biosensors*, vol. 9, 35, 2019.

[9] S. Siyang, C. Wongchoosuk, T. Kerdcharoen, "Diabetes Diagnosis by Direct Measurement from Urine Odor Using Electronic Nose," in *Proc. of Biomedical Engineering International Conference*, BMEiCON 2012, pp. 1-4, 2012.

[10] Airbus Wants its Bomb-detecting 'e-nose' to Sense COVID-19. 2020. Available online at: https://www.laboratoryequipment.com/563979-Airbus-Wants-its-Bomb-detecting-E-nose-to-Sense-Viral-Diseases-Too/ (*last access August 2021*)

[11] P. Jia, F. Tian, Q. He, S. Fan, J. Liu, S. X. Yang, "Feature Extraction of Wound Infection Data for Electronic Nose based on a Novel Weighted KPCA," *Sensors and Actuators B: Chemical*, vol. 201, pp. 555-566, 2014.

[12] N. Peled, M. Koslow, J. Ryan, H. Haick, "Detection of Volatile Organic Compounds in Cattle Naturally Infected with Mycobacterium Bovis, " *Sensors and Actuators B: Chemical*, vol. 171-172, pp. 588-594, 2012.

[13] M. Baietto, A.D. Wilson, D. Bassi, F. Ferrini, "Evaluation of Three Electronic Noses for Detecting Incipient Wood Decay," *Sensors*, vol. 10, pp. 1062-1092, 2010.
[14] A.D. Wilson, "Identification of Insecticide Residues with a Conducting-Polymer Electronic Nose," *Chemical Sensors*, vol. 4, no. 3, pp. 1-10, 2014.
[15] L. Capelli, S. Sironi, R. Del Rosso, "Electronic Noses for Environmental Monitoring Applications," *Sensors*, vol. 14, no. 11, pp.19979-20007, 2014.
[16] C. Wongchoosuk, C. Khunarak, M. Lutz, T. Kerdcharoen, "WiFi Electronic Nose for Indoor Air Monitoring," in *Proc. of International Conference on Electrical Engineering/Electronics, Computer, Telecommunications and Information Technology*, ECTI-CON 2012, pp. 1-4, 2012.
[17] S.M. Mishra, S.H. Saeed, "Optimization of Electronic Sensors for Detecting Pollution due to Organic Gases Using PARAFAC," *International Journal of Electrical and Computer Engineering*, vol. 9, no. 5, pp. 3341-3349, 2019.
[18] R.E. Baby, M. Cabezas, E. de Reca, "Electronic Nose: A Useful Tool for Monitoring Environmental Contamination," *Sensors and Actuators B: Chemical*, vol. 69, pp. 214-218, 2000.
[19] I. Iswanto, A. Maarif, B. Kebenaran, P. Megantoro, "Design of Gas Concentration Measurement and Monitoring System for Biogas Power Plant," *Indonesian Journal of Electrical Engineering and Computer Science*, vol. 22, no. 2, pp. 118-124, 2020.
[20] M.K Ibrahim, N.M. Hussien, S.N. Alsaad, "Smart System for Monitoring Ammonium Nitrate Storage Warehouse," *Indonesian Journal of Electrical Engineering and Computer Science*, vol. 23, no. 1, pp. 583-589, 2021.
[21] L. Wang, Y.H. Gui, S.P. Zhang, "Research on Explosives Detection by Electronic Nose," *Chinese Journal of Sensors and Actuators*, vol. 20, pp. 42-45, 2007.
[22] R.C. Young, W.J. Buttner, B.R. Linnell, R. Ramesham, "Electronic Nose for Space Program Applications," *Sensors and Actuators B: Chemical,* vol. 93, pp. 7-16, 2003.
[23] B Gunawan, S. Alfarisi, G. Satrio, A Sudarmaji, M. Malvin, K. Krisyarangga, "MOS Gas Sensor of Meat Freshness Analysis on E-nose, *TELKOMNIKA*, vol 71, no. 2, pp 771-780, 2019.
[24] D. R. Wijaya, R. Sarno, E. Zulaika, "Gas Concentration Analysis of Resistive Gas Sensor Array," in *Proc. of International Symposium on Electronics and Smart Devices*, ISESD 2016, pp. 337-342, 2016.
[25] M. Gancarz, J. Wawrzyniak, M. Gawrysiak, D. Wiacek, A. Nawrocka, M. Tadla, R. Rusinek, "Application of Electronic Nose with MOS Sensors to Prediction of Rapeseed Quality," *Measurement*, vol. 103, pp. 227-234, 2017.
[26] R. Macias-Quijas, R. Velazquez, N. I. Giannoccaro, A. Lay-Ekuakille, "A Novel Electronic Nose Instrument for the Detection of Volatile Hazardous Compounds: Preliminary Results," in *Proc. of International Conference on Control, Instrumentation and Automation*, ICCIA 2021, pp. 1-5, 2021.
[27] M.R. Wall, D. Neuhauser, "Extraction, Through Filter-Diagonalization, of General Quantum Eigenvalues or Classical Normal Mode Frequencies from a Small Number of Residues or a Short Time Segment of a Signal," *Journal of Chemical Physics*, vol. 102, 8011, 1995.
[28] V.A. Mandelshtam, "FDM: The Filter Diagonalization Method for Data Processing in NMR Experiments," *Progress in Nuclear Magnetic Resonance Spectroscopy*, vol. 38, pp.159-196, 2001.
[29] A. Lay-Ekuakille, C. Pariset, A. Trotta, "Leak Detection of Complex Pipelines Based on the Filter Diagonalization Method: Robust Technique for Eigenvalue Assessment," *Measuremente Science and Technology*, vol. 21, no. 11, 115403, pp. 2010.
[30] A. Lay-Ekuakille, G. Vendramin, A. Trotta, "Robust Spectral Leak Detection of Complex Pipelines Using Filter Diagonalization Method," *IEEE Sensors Journal*, vol. 9, pp.1605-1614, 2010.
[31] V.A. Mandelshtam, H.S. Taylor, "Harmonic Inversion of Time Signals and its Application," *Journal of Chemical Physics*, vol. 107, pp. 6756-6769, 1997.
[32] D.J. Evans, W.S. Yousif, "The QZ Algorithm for the Calculation of the Eigenvalues of a Real Matrix," *Parallel Algorithms and Applications*, vol. 4, pp. 183-192, 1994.
[33] V.M. Alvarez-Pato, C.N Sanchez, J. Dominguez-Soberanes, D.E. Mendoza-Perez, R. Velazquez, "A Multisensor Data Fusion Approach for Predicting Consumer Acceptance of Food Products," *Foods*, vol. 9, no. 6, 774, 2020.
[34] B. Calabrese, R. Velazquez, C. Del-Valle-Soto, R. de Fazio, N.I. Giannoccaro, P. Visconti, "Solar-Powered Deep Learning-Based Recognition System of Daily Used Objects and Human Faces for Assistance of the Visually Impaired," *Energies*, vol. 13, no. 22, 6104, 2020.
[35] P. Visconti, R. Velazquez, S. Capoccia, R. de Fazio, "High-Performance AES-128 Algorithm Implementation by FPGA-based SoC for 5G Communications," *International Journal of Electrical and Computer Engineering*, vol. 11, no. 5, pp. 4221-4232, 2021.
[36] C. Del-Valle-Soto, L.J. Valdivia, R. Velazquez, L. Rizo-Dominguez, J.C. Lopez-Pimentel, "Smart Campus: An Experimental Performance Comparison of Collaborative and Cooperative Schemes for Wireless Sensor Network," *Energies*, 12, 3135, 2019.
[37] P. Visconti, N.I. Giannoccaro, R. de Fazio, S. Strazzella, D. Cafagna, "IoT-Oriented Software Platform Applied to Sensors-based Farming Facility with Smartphone Farmer App," *Bulletin of Electrical Engineering and Informatics*, vol. 9, no. 3, pp. 1095-1105, 2020.